Wetlands (2015) 35:745–756
DOI 10.1007/s13157-015-0666-y

ORIGINAL RESEARCH

Wetlands of the Lowland Amazon Basin: Extent, Vegetative Cover, and Dual-season Inundated Area as Mapped with JERS-1 Synthetic Aperture Radar

Laura L. Hess[1] · **John M. Melack**[1] · **Adriana G. Affonso**[2] · **Claudio Barbosa**[2] · **Mary Gastil-Buhl**[3] · **Evlyn M. L. M. Novo**[2]

Received: 25 November 2014 / Accepted: 28 May 2015 / Published online: 20 June 2015

Abstract Wetland extent, vegetation cover, and inundation state were mapped for the first time at moderately high (100 m) resolution for the entire lowland Amazon basin, using mosaics of Japanese Earth Resources Satellite (JERS-1) imagery acquired during low- and high-water seasons in 1995–1996. A wetlands mask was created by segmentation of the mosaics and clustering of the resulting polygons; a rules set was then applied to classify wetland areas into five land cover classes and two flooding classes using dual-season backscattering values. The mapped wetland area of 8.4×10^5 km^2 is equivalent to 14 % of the total basin area (5.83×10^6 km^2) and 17 % of the lowland basin (5.06×10^6 km^2). During high-water season, open water surfaces accounted for 9 % of the wetland area, woody vegetation 77 %, and aquatic macrophytes 14 %. Producer's accuracy as assessed using high-resolution digital videography was better than 85 % for wetland extent. The mapped flooding extent is representative of average high- and low-flood conditions for latitudes north of 6° S; flooding conditions were less well captured for the southern part of the basin. Global data sets derived from lower-resolution optical sensors capture less than 25 % of the wetland area mapped here.

✉ Laura L. Hess
lola@eri.ucsb.edu

[1] Earth Research Institute, University of California, Santa Barbara, USA

[2] Remote Sensing Division, National Institute for Space Research (INPE), São José dos Campos, Brazil

[3] Marine Science Institute, University of California, Santa Barbara, USA

Keywords Tropical wetlands · Amazon River · Floodplain inundation · Radar remote sensing · JERS-1 · Global Rain Forest Mapping Project

Introduction

Freshwater ecosystems play an important role in global hydrologic and carbon cycles (Alsdorf et al. 2003; Cole et al. 2007), provide a wide range of ecosystem services including fish and fiber production, water supply, water purification, and flood regulation (Acreman and Holden 2013), and are rich in species diversity and endemism (Revenga et al. 2005). Freshwater habitats are also among the most threatened by human activities and by climate change (Abell 2002; Kingsford 2011; Castello et al. 2013). Despite their importance, the extent of inland waters and adjacent wetlands, and the temporal variability of surface waters, are not well characterized (Alsdorf et al. 2003; Downing 2009), limiting our ability to monitor and manage freshwater ecosystems at watershed scale (Finlayson et al. 2005) and to incorporate freshwater ecosystems into land surface models at global scale (Wood et al. 2011). Since the inception of the Ramsar Convention on Wetlands in 1971, Contracting Parties have been called upon to prepare national wetland inventories; yet only one third of Ramsar Parties had initiated a national inventory process as of 2009 (Lowry et al. 2009). Mapping technologies that can aid in delineating and characterizing wetlands over large regions are urgently needed.

Remotely sensed imagery from optical sensors such as Landsat Thematic Mapper, SPOT, QuickBird, and Ikonos has been widely used for regional wetlands mapping (Ozesmi and Bauer 2002; Adam et al. 2010). In the humid tropics, however, the task of assembling cloud-free coverage over large areas during the seasons corresponding to phases of

the flood cycle is challenging. While optical sensors with high temporal resolution such as MODIS can be used to monitor flooding and phenology in some types of large wetlands (Orodyne and Friedl 2008; Landmann et al. 2010), their spatial resolution (250 m–1 km) is insufficient for smaller streams and wetlands, and flood detection within woody stands is limited to those with low canopy cover. Global land cover data sets derived from these sensors typically include few or no wetland classes other than open water, and consistency among global 1-km land cover data sets is low for water-related land cover types (Nakaegawa 2012).

L-band synthetic aperture radar (SAR) sensors – active imaging systems operating in the 1–2 GHz range (15–30 cm) – are well suited to large-scale land cover mapping in tropical regions because of their ability to penetrate clouds and to distinguish among woody, herbaceous, and non-vegetated cover (Kasischke et al. 1997). Water, herbaceous vegetation, and forest present increasingly rough targets to L-band radars, resulting in higher backscattering and image tones ranging from black (water) to dark gray (herbaceous) and medium gray (forest) (Fig. 1). L-band SAR systems in HH mode (horizontal send and receive polarization) are particularly useful for mapping wetlands because they can reliably detect flooding beneath most vegetation canopies (Hess et al. 1990; Melack 2004). Specular reflections from sub-canopy water surfaces undergo a second ("double-bounce") reflection against tree trunks or larger herbaceous stalks, enhancing backscattering and resulting in bright image tones (Wang et al. 1995; Silva et al. 2008). Although the L-HH backscattering signatures of vegetation cover types are not unique, temporal changes in backscattering linked to seasonal variability in flooding state significantly improves separability of classes (Hess et al. 2003; Arnesen et al. 2013). SAR-based mapping of tropical wetlands has been done for a few large regions such as the Brazilian Pantanal (Evans et al. 2010) and the island of Borneo (Hoekman et al. 2010), but so far has not been applied at basin-wide scale for the world's largest river basin, the Amazon.

During the 1990s, mosaics of L-band SAR data from the Japanese Earth Resources Satellite 1 (JERS-1) were assembled for tropical and boreal regions as part of the Global Rain Forest Mapping (GRFM) Project (Rosenqvist et al. 2000). As part of a Large-Scale Biosphere-Atmosphere Experiment in Amazonia (LBA; Keller et al. 2013) study, Hess et al. (2003) mapped and validated wetland extent, vegetative cover, and flooding state for an 18°×8° portion of the central Amazon using dual-season GRFM mosaics. Here we extend the LBA wetlands mapping to report the first validated estimate of wetland extent, cover, and flooding for the lowland Amazon basin. We describe mapping and validation methods and results, discuss the timing of the two mosaics relative to regional precipitation and discharge records, and compare mapped areas with estimates from global and regional land cover data sets.

The thematic scope of the mapping includes all surface waters, incorporating lakes, rivers, and wetlands; these linked ecosystem types we refer to collectively as "wetlands". This usage, though somewhat unconventional, corresponds with the Ramsar definition of wetlands (Scott and Jones 1995) and acknowledges the importance of linkages among different

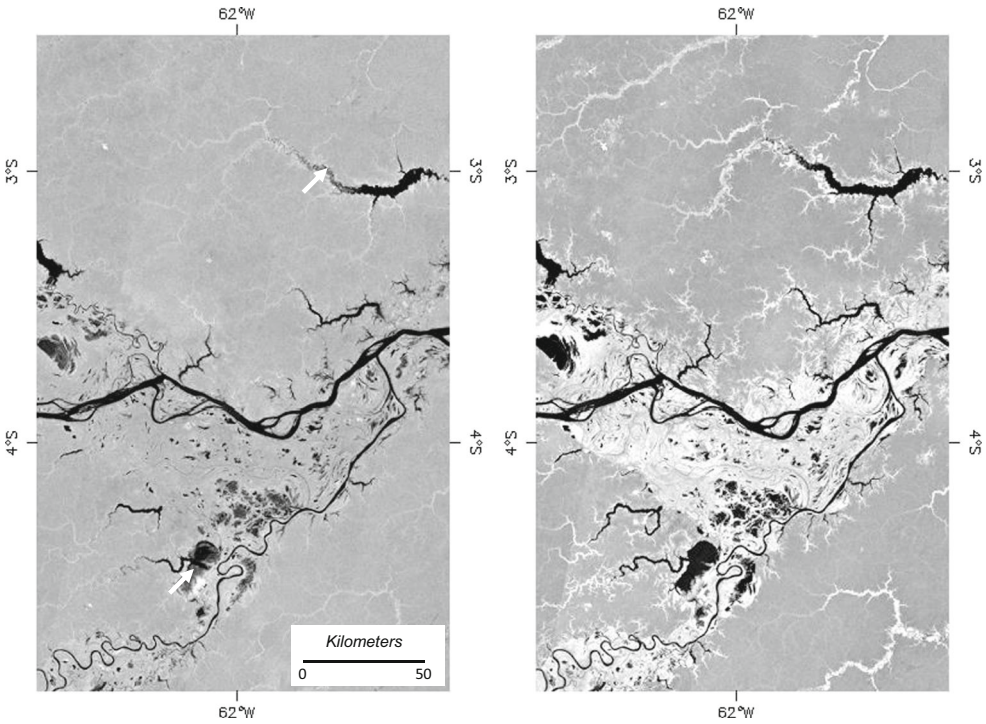

Fig. 1 Example of low-water (*left*) and high-water (*right*) GRFM mosaics of JERS-1 SAR images for region near the confluence of the Purus and Solimões (Amazon) rivers. Seasonally flooded forests appear *gray* in their non-flooded state at left (Oct.-Nov. 1995), and white in their flooded phase at right (May-July 1996), when double-bounce reflections enhance SAR returns. *Arrows* indicate areas where shrubs or short trees are exposed at low water (*dark gray* on scene at left) and submerged at high water (*black* on scene at right, indicating open water). © JAXA, METI

types and hierarchical scales of freshwater ecosystems (Lamberti et al. 2010). It also recognizes that on floodplains of large tropical rivers, the aquatic-terrestrial transition zone migrates as a function of the river flood pulse (Junk et al. 1989; Bayley 1995), so that delineations of channels, lakes, and floodplains vary seasonally.

Methods

Study Area and Satellite Data

JERS-1 scenes acquired during Oct.-Nov. 1995 and during May-July 1996 were used for the wetland mapping. Scenes were radiometrically calibrated and mosaicked at 3-arcsecond pixel size (approximately 90 m) to create the dual-season GRFM Amazon mosaics (Siqueira et al. 2000; Chapman et al. 2002). The two mosaics are refered to as "low-water" (1995) and "high-water" (1996) based on their correspondence to low-flood and high-river stages in the central basin. GRFM mosaic geolocation was based on tie-points located in regions for which 1:100,000 or larger-scale maps were available, resulting in a lack of tie-points and impaired geolocation for some portions of the basin. For our analysis, geolocation was refined using 180 additional tie-points located on the 1990s-era GeoCover™ Orthorectified Landsat Thematic Mapper Mosaics (Earth Satellite Corporation 2002). Tie-points were restricted to flat areas, and no attempt was made to correct terrain distortions resulting from SAR geometry. Such terrain distortions affect hilly and mountainous areas, and do not degrade geolocation in the lowland floodable areas that are the focus of this study.

The area mapped was the lowland Amazon, defined as the portion of the Amazon watershed below 500 m asl (Fig. 2). Using Shuttle Radar Topography Mission (SRTM) digital terrain elevation data (Farr et al. 2007; Jarvis et al. 2008), areas greater than or equal to 500 m asl were excluded. The RiverTools software package (Peckham 2008) was used to delineate watersheds of the Amazon and its major tributaries, setting the Amazon basin outlet where the mainstem Amazon River channel splits into north and south channels west of Gurupá Island (51.4375° W, 0.4583° S). This Amazon watershed delineation excludes the Tocantins watershed as well as most of Marajó Island and adjacent islands of the Amazon estuary, regions grouped together with the Amazon basin in some studies. The resulting study area of 5.06×10^6 km^2 is 87 % of the total basin (5.83×10^6 km^2). The GRFM mosaics did not include portions of Bolivia south of 16° S and Brazil north of 4°N; as described below, these regions were mapped using a combination of radar and optical imagery.

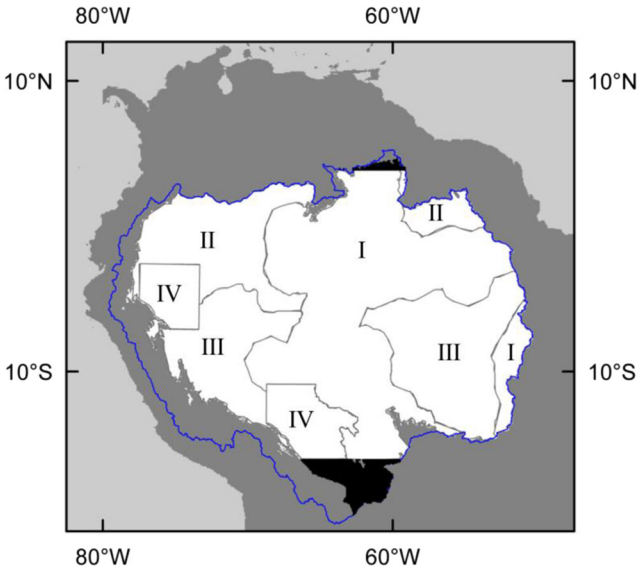

Fig. 2 Study area within which wetland areas were mapped using GRFM mosaics (*white*); Amazon basin boundary (*blue*); and validation regions. *Black areas* were mapped using PALSAR and Landsat mosaics. *Gray areas* within basin are greater than 500 m asl

Wetland and Land Cover Class Definitions

Although there is widespread agreement that the term "wetland" refers to habitats with continuous, seasonal, or periodic standing water or saturated soils, specific criteria for designating a particular site as a wetland vary regionally and depend on the intended application (Finlayson and van der Valk 1995; Scott and Jones 1995). The wetlands mapping described here is intended primarily for large-region biogeochemical and hydrologic modeling of lowland Amazon wetlands with seasonal or permanent standing water. For these applications, key information requirements are 1) status as wetland or non-wetland, 2) vegetation structural type, and 3) flooding state during the local flooded and nonflooded seasons. While these criteria are not sufficient for discriminating all wetland types specified by comprehensive classification systems for Amazonian wetlands such as that of Junk et al. (2011), they provide a starting point for deriving these classes at basin-wide scale.

For this study, wetland areas were defined as (1) areas that were inundated on either or both radar mosaics and (2) areas not flooded on either date, but adjacent to flooded areas and displaying landforms consistent with wetland geomorphology. The second condition is necessary since the two mosaic acquisition periods did not capture high-water conditions for all parts of the basin. Classification of areas under condition 1 was automated, while condition 2 required hand editing by trained interpreters. Under condition 2, a conservative approach was taken; ambiguous cases were thus not included as wetland areas. Seasonally or permanently saturated areas with hydromorphic soils or wetland vegetation are not necessarily detectable using L-band SAR. However, in the humid tropics, these areas are likely to have at least discontinuous

pools of standing water during the rainy season, allowing detection. River channels and permanent lakes and reservoirs are included here within the definition of wetland areas.

The wetland definition used here is not date-specific, since in addition to automated detection of water and flooded vegetation on specific dates it employed human interpretation of features that were judged likely to be flooded on other dates (condition 2). The land cover and inundation mapping, however, was date-specific, labeling what can be termed "land cover states" composed of five land cover types (nonvegetated, herbaceous, shrub, woodland, forest) and two flooding states (nonflooded, flooded). The nonvegetated class is equivalent to bare ground (e.g., sand bar or mud bank) when nonflooded, and to open water when flooded. The flooded herbaceous class includes both emergent flooded plants and floating beds of aquatic vegetation, but omits submerged aquatic plants, which cannot be detected with SAR. The date-specific approach allows consideration of temporal transitions that are common in Amazonian wetlands, such as from nonflooded shrub to open water (as the shrubs are submerged), or from flooded herbaceous to open water (as floating aquatic macrophytes senesce and decompose, or are dislocated by wind or current).

Definitions of the five land cover types follow conventions of the UN-FAO Land Cover Classification System (LCCS) (Di Gregorio 2005). Woody vegetation is partitioned between tree and shrub using a height limit of 5 m. Forests are areas with tree canopy cover of more than 70 %, while areas with 20 % to 70 % tree cover are classed as woodlands. In this study, only shrublands with closed canopy cover (>70 %) are considered. Under the LCCS guidelines, nonvegetated areas have<4 % vegetative cover. This definition was modified to include as nonvegetated any areas with sparse (4 to 20 %) canopy cover. These vegetation height and canopy cover criteria were applied in labeling training and validation samples from high-resolution digital videography.

Classification of SAR Mosaics

A wetlands mask was created by segmentation of the SAR mosaics and clustering of the resulting polygons based on mean backscattering coefficient (σ°) (Hess et al. 2003). Region-growing segmentation and iterative clustering into wetland and non-wetland classes were performed using the SPRING software package (Câmara et al. 1996). Since high-resolution digital terrain data were not available at the time the SAR mosaics were generated, no terrain correction had been applied to modify backscattering based on local incidence angles. The high returns from facing slopes closely resembled those from flooded forest. These areas, and human-impacted areas such as roads which had returns similar to those from rivers, were removed from the wetland mask by manual editing. The minimum mapping unit was approximately 1 km^2; however, continuous linear features could include segments as narrow as 1 pixel (approx. 100 m).

Within the wetlands mask, a rule set (Hess et al. 2003) was applied on a per-pixel basis to classify wetland areas into the five land cover classes and two flooding classes based on dual-season σ° values. Dual-season backscattering signatures for shrub and aquatic macrophyte classes were not unique, resulting in high confusion rates when a single rules set was applied basin-wide. Confusion rates between open water and bare ground surfaces were similarly high, owing partly to the high noise floor of the JERS-1 instrument (Chapman et al. 2002). Three regional rules sets were therefore used, modifying shrub/macrophyte and bare-soil/water decision thresholds based on a priori expectation of the classes for 1) floodplains inundated primarily by whitewater, where aquatic macrophytes were more likely to occur than shrubs; 2) floodplains, interfluvial swamps, and reservoirs inundated primarily by blackwater or direct precipitation, where shrubs were more likely to occur than aquatic macrophytes; and 3) the Llanos de Moxos, Roraima, and Humaitá savannas, where confusion between bare surfaces and water was likely to result in overestimation of open water.

The above-described methods were applied to the latitudinal range covered by the GRFM mosaics (4° N to 16° S). In order to provide a complete mapping for the lowland Amazon basin, wetlands north and south of this range (3 % of the total lowland Amazon) were mapped using a combination of 1) dual-polarization ALOS PALSAR mosaics from 2007 to 2010 (Shimada et al. 2014; downloaded from http://www.eorc.jaxa.jp/ALOS/en/palsar_fnf/fnf_index.htm) and 2) mosaics of Landsat images from 2011 (Hansen et al. 2013; downloaded from http://earthenginepartners.appspot.com/science-2013-global-forest/download_v1.1.html). Although these data sets do not include the date-specific flooding information provided by the GRFM mosaics, the combination of optical and radar data, and the cross-polarized (HV) band available for PALSAR, compensate somewhat for the lack of seasonal information. The Landsat and PALSAR mosaics (resampled to the GRFM 3-arcsecond pixel size) were classified using a method analogous to that applied to the GRFM mosaics, except that dual-season classes for these wetlands were inferred based on the strength of the flooding signal. For example, wetland forests with very bright returns were classified as flooded during both high- and low-water seasons and those with moderately bright returns were classified as seasonally flooded. The Bañados del Izozog, an important wetland of the Bolivian Chaco, could not be clearly delineated using the PALSAR and Landsat mosaics owing to highly seasonal or intermittent flooding patterns; wetland boundaries and vegetation structure were therefore delineated with reference to Navarro and Fuentes (1999) for this region.

Accuracy Assessment

Accuracy assessment included three interrelated elements: geolocation accuracy, thematic accuracy, and representativeness of average flooding patterns. The stated uncertainty for

the GeoCover data set, combined with the RMS error for test points following coregistration of the SAR mosaics with GeoCover, yields an estimated geolocation error of 75 m, with a maximum error of 300 m. A 1999 airborne campaign acquiring high-resolution digital videography, and timed to correspond seasonally to the May-July 1996 mosaic acquisition period (Hess et al. 2002), was the primary validation data set for thematic accuracy. Because flight lines were limited to Brazil and cannot be considered representative of the entire study area, sub-regions within the GRFM study area were designated as one of four thematic accuracy zones (Fig. 2).

Zone I is a 500-km buffer zone centered on the 1999 videography flight lines. Within this zone, videography-based accuracy statistics should be valid. Beyond this buffer zone, the applicability of the videography-based results depends on whether the vegetation types and flooding conditions in those regions were represented within the videography data set. The remainder of the study area was subdivided into regions where both vegetation and flood conditions were likely to be represented (zone II), and those where either vegetation or flood timing was not well represented in the video data set (zone III). For extensive wetlands in the Marañon-Ucayali region of Peru and for the Llanos de Moxos in Bolivia (Zone IV), accuracy was assessed by comparison with recent high-resolution vegetation maps (Josse et al. 2007). Accuracy was not assessed for the 3 % of the study region not covered by the GRFM mosaics.

Validation samples for Zones I and II were selected by random sampling of flight time codes, each of which was associated with a 100×100 m (1 ha) sample at the center of a geotiff file extracted from the videography. Samples with wetland cover occupying<10, 10–90, or>90 % of the 1 ha sample were labeled as Nonwetland, Mixed, or Wetland, respectively. Samples labeled as Wetland were further labeled according to the dominant land cover as Open Water, Herbaceous, Woody, or Mixed.

Timing of the JERS-1 mosaics relative to typical flooding patterns was assessed by comparing the seasonality of precipitation and river discharge with the acquisition dates of the scenes composing the GRFM mosaics. Timing of maximum and minimum rainfall for the period 1961–1990 was derived from the 0.5° gridded Climatic Research Unit TS 2.1 data set (Mitchell and Jones 2005). Timing of river discharge for 78 stations in Brazil was derived from the data set of Costa et al. (2002); timing for three stations in Peru was determined from hydrographs provided online by the Servicio Nacional de Meteorología y Hidrología del Peru (SENAMHI Peru, n.d.).

Results and Discussion

Wetland Area, Cover, and Inundation State

Our dual-season mapping (Fig. 3) found a wetland area of 8.4×10^5 km^2 for the lowland Amazon (Table 1), which represents 14 % of the total basin area (5.83×10^6) and 17 % of the lowland basin (5.06×10^6). Open water constituted 7 % of the wetland area on the Oct-Nov 1995 mosaic and 9 % on the May-July 1996 mosaic (5.6×10^4 and 7.3×10^4 km^2, respectively). At high-water stage, woody vegetation (forest, woodland, shrub) covered 77 % of the wetland area, while herbaceous vegetation (aquatic macrophyte at high water) occupied 14 %. The flooded portion of the wetland area varied from 34 % during Oct.-Nov. 1995 to 75 % during May-July 1996. The flooded portion varied from 5 to 11 % relative to the entire Amazon watershed, and from 6 to 13 % relative to the

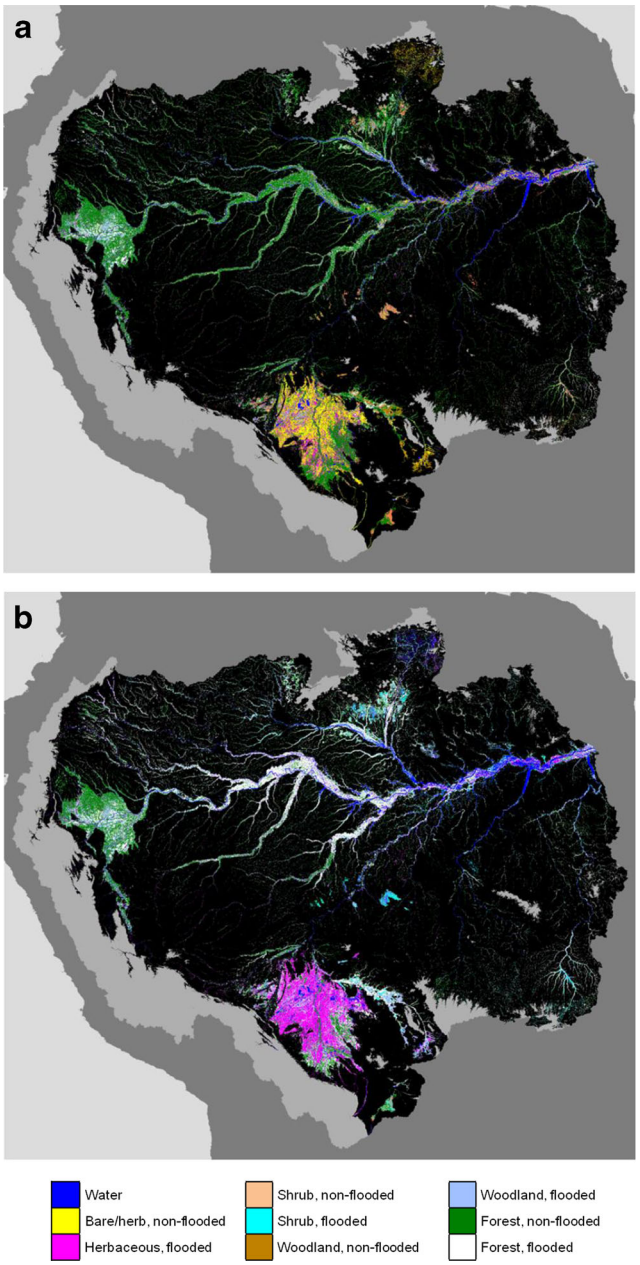

Fig. 3 **a** Amazon wetland classes mapped during Oct.-Nov. 1995 (low water) and **b** May-June 1996 (high water). *Black areas* are non-wetland and *gray areas* within the Amazon basin have elevations greater than 500 m

Table 1 Mapped areal extent ($km^2 \times 1000$) of Amazon wetland cover classes and inundation states

	Low-water, Oct.-Nov. 1995			High-water, May-July 1996		
Cover class	Non-flooded	Flooded	Total	Non-flooded	Flooded	Total
Open water	0.0	56.3	56.3	0.0	73.2	73.2
Herbaceous/bare	79.0	52.8	131.8	0.0	120.2	120.2
Shrub	46.5	3.0	49.5	1.2	42.9	44.1
Woodland	19.0	67.8	86.8	0.0	86.8	86.8
Forest	411.2	105.3	516.4	204.9	311.5	516.4
Total	555.6	285.2	840.8	206.1	634.6	840.8

lowland portion of the basin. All wetland areas were not simultaneously flooded on the high-water (1996) mosaic because of regional differences in timing of flooding. Brazil accounts for about half (52 %) of the Amazonian wetland area, with large areas also present in Bolivia (24 %) and Peru (17 %), and small areas in Colombia (4 %), Venezuela (1 %), and Guyana (<1 %). Forty-four percent of the wetland area is located within the watersheds of the two largest tributaries of the Amazon, the Madeira and Negro rivers (Table 2). The Marañon sub-basin has the highest proportion of total area as wetland (20 %), followed by the Madeira (19 %) and Içа-Putumayo (17 %). The sub-basins with the smallest proportion as wetland are the Tapajós (5 %) and the Xingu (8 %).

The transitions in cover states between the two flooding seasons (for wetlands within the GRFM region; Table 3) fall into three groups. 1) Sixty-two percent of the wetland pixels did not change in either cover type or flooding state between the two dates (although the pixels flooded both dates would have been flooded more deeply at high water). These included (semi)-permanently flooded areas of all cover types, forested areas not flooded on either date because the local flood peak did not correspond to the imaging dates, and forested areas on high levees that do not flood every year. The shrubs in this group are tall enough relative to the local flood amplitude that they are not submerged at high water. (Semi)-permanently flooded woody vegetation covers an area of 1.99×10^5 km^2, or 25 % of the total wetlands; about half of this is forest. 2) Pixels that transitioned from non-flooded to flooded without a change in cover type accounted for 35 % of the total area; this group includes seasonally flooded forest, seasonal aquatic macrophyte stands with bare soil or terrestrial phase grass cover at low water, and seasonally flooded shrubs. 3) For the remaining 3 % of the wetland pixels, cover type changed between seasons. These are primarily shrub or herbaceous areas covered by open water at high flood stage, plus some areas that transition from open water to aquatic macrophyte.

Thirty-eight percent of the mapped wetlands were flooded on both dates, 37 % on only one date, and 25 % on neither date. Areas occupied by open water on both mosaics, corresponding to river channels and permanent to semi-permanent lakes, cover 0.53×10^5 km^2, less than 7 % of the total wetland area. Of the 1.04×10^5 km^2 with macrophyte cover at some time of year, 52 % was dry (bare or non-flooded herbaceous) at low-water stage, and 42 % had (semi)-permanent macrophyte cover; only 6 % transitioned from open water to macrophyte. Aquatic macrophyte stands, particularly floating grasses, may shift position during the growing season (Silva et al. 2010); the complexity of this type of transition between cover states is not captured here.

Assessment of Thematic Accuracy

From a pool of 748 labeled videography samples, validation data sets were created by random selection from Nonwetland

Table 2 Wetland area ($km^2 \times 1000$) within watersheds of major tributaries

Tributary watershed	Wetland area	Watershed area	Percent of tributary watershed	Percent of Amazon wetlands
Madeira	254.6	1317.4	19.3	30.3
Negro	117.1	721.5	16.2	13.9
Marañon	70.9	358.4	19.8	8.4
Ucayali	41.5	356.3	11.7	4.9
Xingu	37.1	492.1	7.5	4.4
Purus	36.1	368.2	9.8	4.3
Japurá-Caquetá	31.9	255.9	12.5	3.8
Tapajós	22.2	492.2	4.5	2.6
Juruá	20.9	189.3	11.0	2.5
Içа-Putumayo	20.3	117.9	17.2	2.4

Table 3 Transitions in cover states (km^2 x 1000) between low- and high-water seasons (*OW* open water, *Hrb* Bare or herbaceous, *Shr* Shrub, *Wdl* Woodland, *For* Forest, *Fl* Flooded, *Nfl* Not flooded); the cases on the diagonal, shown in bold, did not change cover state or flooding state

		High-water cover state								
		OW-Fl	Hrb-Nfl	Hrb-Fl	Shr-Nfl	Shr-Fl	Wdl-Fl	For-Nfl	For-Fl	Total
Low-water cover state	OW-Fl	**53.4**		5.9						59.3
	Hrb-Nfl	11.3		54.7						66
	Hrb-Fl			**43.5**						43.5
	Shr-Nfl	5.2				42.2				47.4
	Shr-Fl	2.4				**11.7**				14.1
	Wdl-Fl						**78.1**			78.1
	For-Nfl							**196.6**	184.6	381.2
	For-Fl								**109.3**	109.3
	Total	72.3	0	104.1	0	53.9	78.1	196.6	293.9	798.9*

[a] Transitions are tabulated here only for wetlands covered on the dual-season GRFM mosaics (latitudes 4 °N to 16°S)

and Wetland samples to assess the accuracy of the wetland area mapping, and from Wetland samples to assess the accuracy of the vegetation classes mapped at high-water stage. Percent accuracy (producer's, user's, and overall) and Kappa coefficients are shown in Table 4. Overall accuracy was good for both the wetland mapping (93 % accurate) and vegetation mapping (86 % accurate). Producer's accuracies were good for all categories except herbaceous (equivalent to aquatic macrophyte at high-water stage) and open water. The low accuracy of 50 % for macrophytes resulted primarily from the similarity in backscattering coefficient among macrophytes, nonflooded forest, nonflooded shrubs, and barely emergent flooded shrubs. Accuracy for macrophytes in this study was lower than the 65 % reported by Hess et al. (2003) because that study targeted areas with relatively less shrub cover. The 78 % accuracy for water was lower than what is normally expected for open water using L-band SAR. The high noise equivalent σ° for JERS-1 (approximately −18 dB for the GRFM mosaics; Chapman et al. 2002) resulted in misclassification of some water pixels as bare ground, especially in savanna regions with sparse vegetation, such as Roraima. However, much of the error for this class was likely due to actual differences in cover between map and reference samples, e.g., samples having macrophyte cover during the 1999 videography flight but not on the 1996 JERS-1 image, or shallow, seasonally flooded ponds that were dry in 1999.

Table 4 Videography-based thematic accuracy assessment (applicable to Zones I, II): wetland/ nonwetland and water/herbaceous/woody

	Producer's accuracy (%)	User's accuracy (%)
Wetland (floodable) and nonwetland areas		
Nonwetland	93.9	98.7
Wetland	88.3	69.7
Overall Accuracy: 93.2 %		
Kappa coefficient: 0.740		
Vegetation cover at high-water stage		
Open water	78.1	95.0
Herbaceous	50.0	36.0
Woody	95.5	92.0
Overall accuracy: 86.2 %		
Kappa coefficient: 0.743		

For Zone IV, high-resolution ecological systems maps of the Peruvian and Bolivian Amazon (Josse et al. 2007) were reprojected and masked to correspond with the JERS-1 mosaics, and all mapped classes subject to inundation were combined to create a validation data set for the wetland mask. Comparison of all pixels within Zone IV showed a correspondence rate of 90 % for Peru and 76 % for Bolivia. The lower agreement rate for Bolivia resulted largely from the present study's misclassification as non-wetland of areas that were not flooded during either mosaic imaging period.

Hydrologic Representativeness of Mosaics

In order to estimate the degree to which the "high-" and "low-" water mosaics represent typical flooding conditions, the month of JERS-1 acquisition for the low- and high-water mosaics was first compared to the month of minimum and maximum precipitation. This comparison (Fig. 4) is most relevant for small rivers, interfluvial wetlands, and portions of savanna wetlands, where direct precipitation, runoff from local watersheds, and water table levels drive flooding patterns.

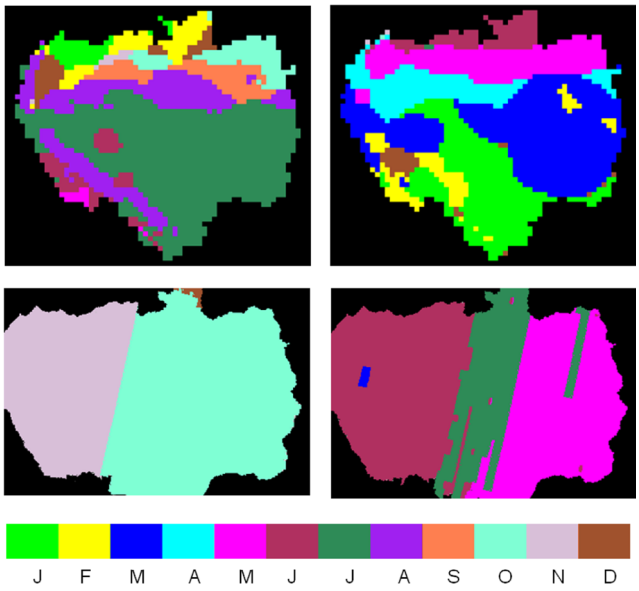

Fig. 4 Upper: month of minimum (*left*) and maximum (*right*) precipitation. Lower: Acquisition month of JERS-1 low-water (*left*) and high-water (*right*) imagery composing GRFM mosaics

For much of the basin south of about 6° S, the driest months occur from July to August and the wettest months from December to March. For these areas, dry-season inundation may be overestimated, and wet-season inundation underestimated, based on the JERS-1 mosaics. For the northern part of the basin, timing of minimum precipitation is similar to that of the low-water mosaic except for areas north of the equator and west of 60°, while timing of maximum precipitation is within 1 month of the JERS-1 high-water acquisitions.

On large river floodplains, inundation is driven by changes in river stage; the river flood pulse spreads to the floodplain primarily via distributive floodplain channels and overbank flow from the main river channel. A second hydrologic assessment of the mosaic compared peak river stage with timing of the JERS-1 1996 mosaic. This comparison (Fig. 5) reveals timing offsets of −1 to +1 month for most gauges north of 4° S, +2 months for most of the southeastern part of the basin, and +2 to +4 months for the south-central basin (roughly 62° W to 73° W), where a positive offset indicates stage peak preceding JERS-1 1996 acquisitions. The effect of such offsets on estimates of maximum flooded area depends on the residence time of floodwaters in the inundated areas. For larger rivers, residence time is generally sufficient that underestimation of maximum flooded area due to imaging 1–2 months following peak flood stage is relatively minor. Offsets of 3–4 months, however, are likely to result in significant underestimation.

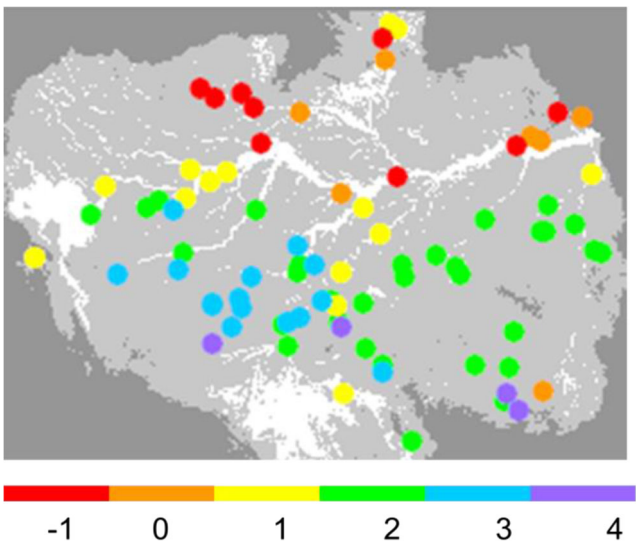

Fig. 5 Number of months by which JERS-1 high-water acquisition date preceded (*negative numbers*) or lagged (*positive numbers*) the mean month of peak river discharge for 81 gauging stations

Comparison with Global Data Sets

We compared our results (which we refer to as the LBA wetlands mapping) to wetlands and water classes from two vector and five raster products (Table 5). Three raster products were derived from 0.5- to 1-km resolution optical data: the MODIS Yearly L3 Global 500 m Land Cover Type Product (MCD12Q1: Friedl et al. 2002), the Global Land Cover Characterization (GLCC: Loveland et al. 2000), and the Joint Research Centre Global Land Cover 2000 (GLC 2000: Eva et al. 2002). Of the five classification schemes used in the MODIS product, only the IGBP scheme, which includes a Permanent Wetlands class, was evaluated since the other schemes include only water. For comparison with GLCC (South America), the Inland Water class was combined with the five lowland wetland classes (Moist Tropical Evergreen Rainforest/Flooded Tropical Evergreen Rainforest (Mangroves Along Coast), Flooded Grassland/Fragmented Forest and Mangroves, Seasonally Flooded Savanna with Palms, Wooded Wetlands, and Flooded Evergreen Broadleaf Rainforest (Varzea)). Grouped GLC 2000 wetland classes were Mangroves, Fresh Water Flooded Forests, Permanent Swamp Forests, Periodically Flooded Savannah, Periodically Flooded Shrublands, and Water Bodies. The fourth raster product, Global Distribution of Wetland Ecosystems at 1° by 1° resolution (Matthews and Fung 1987), was based on soil, vegetation, and other maps, while the fifth raster product, the Global Lakes and Wetlands GLWD-3 data set (Lehner and Döll 2004) synthesizes a variety of raster and vector data sets including satellite-based mapping. The SRTM Water Body data files (Anonymous 2005) provide near-global vector-formatted river and lake boundaries, and the GLWD-1 and GLWD-2 vector data sets show lakes, rivers, and reservoirs based on source data at 1:1 to 1:3 million scale (Lehner and Döll 2004). The cross-product comparison did not include the regions north and south of the dual-season GRFM mosaics.

Table 5 Comparison of wetland and open water areas ($km^2 \times 10^3$) from the LBA wetlands mapping (this study) with the equivalent region from global land cover data sets

Product	Source data	Grid cell size	Dates	Wetland area[h] ($km^2 \times 10^3$)	Open water[h] ($km^2 \times 10^3$)
LBA wetlands mapping "Low"-water [a]	GRFM JERS-1 mosaic	3 arcsec (~100 m)	Oct-Nov 1995	800	60
LBA wetlands mapping "High"-water [a]	GRFM JERS-1 mosaic	3 arcsec (~100 m)	May-Jul 1996	800	70
SRTM Water Body[b]	SRTM	Vector[i]	Feb 2000	NA	70
MODIS Land (IGBP)[c]	MODIS	500 m	2001	90	40
GLCC (Vers.2) SASLCR[d]	AVHRR	1 km	1992–1993	210	120
GLC 2000[e]	SPOT4, JERS-1, ATSR-2, DMSP	1 km	2000	310	60
Matthews and Fung 1987[f]	Multiple	1°	Various	100	NA
GLWD-1 + GLWD-2[g]	Multiple	Vector[j]	Various	NA	108
GLWD-3[g]	Multiple	30 arcsec (~1 km)	Various	477	94

[a] This paper, based on Global Rain Forest Mapping Project JERS-1 mosaics. Does not include regions north of 4° N or south of 16° S. https://daac.ornl.gov/cgi-bin/dataset_lister.pl?p=11 (LBA-ECO LC-07)

[b] Shuttle Radar Topography Mission (SRTM) Water Body Data Files. http://dds.cr.usgs.gov/srtm/version2_1/SWBD/

[c] Land Cover Type Yearly L3 Global 500 m (MCD12Q1 V005), IGBP legend (Friedl et al. 2002). https://lpdaac.usgs.gov/products/modis_products_table/mcd12q1

[d] Global Land Cover Characterization v. 2, So. Amer. Seasonal Land Cover Regions legend (Loveland et al. 2000). http://edc2.usgs.gov/glcc/sa_int.php

[e] Joint Research Centre Global Landcover 2000, South America (Eva et al. 2002). http://bioval.jrc.ec.europa.eu/products/glc2000/products.php

[f] Global Distribution of Wetland Ecosystems at 1°×1° Resolution (Matthews and Fung 1987). http://data.giss.nasa.gov/landuse/wetland.html

[g] Global Lakes and Wetlands Database (Lehner and Döll 2004). http://www.worldwildlife.org/pages/global-lakes-and-wetlands-database

[h] For the LBA, MODIS, GLCC, GLC2000, and GLWD-3 data sets, Open Water is the subset of Wetland Area comprising rivers, lakes, and reservoirs; Wetland Area includes Open Water and other wetland types

[i] Derived from source data with 3 arcsec (~100 m) cell size

[j] Derived from multiple data sources with scales of 1:1 million to 1:3 million

Estimates of wetland area, including inland water, for the MODIS and GLCC data sets were 90×10^3 and 210×10^3 km^2, or 11 and 26 % of the area derived in this study for the region within the GRFM mosaics. The MODIS estimate is predictably low since the IGBP legend includes only permanently inundated wetlands and open water. As illustrated in Fig. 6 (upper panel), the omission of seasonally inundated wetlands results in much lower estimates of total wetland area. Differences between the LBA and GLCC maps were primarily in closed-canopy forested wetlands, in which optical sensors cannot detect flooding beneath the canopy (although they may detect phenologic signals associated with flood-deciduous species). Low correspondence between GLCC products and higher resolution reference data sets has also

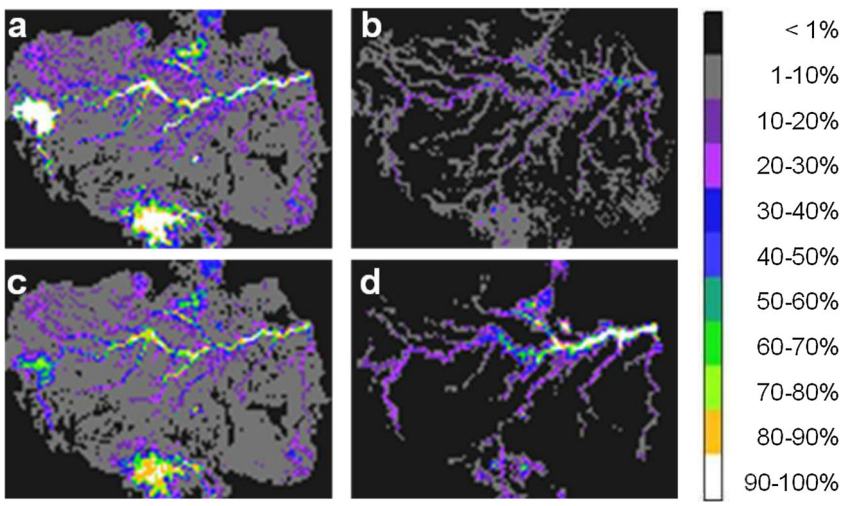

Fig. 6 Upper: Fractional wetland area for 0.25° cells from **a**) LBA wetlands mapping (this paper) and **b**) MODIS Land Cover, IGBP legend. *Lower*: Fractional inundation, May-June 1996 from **c**) LBA wetlands mapping and **d**) coarse-scale multi-satellite observations (Prigent et al. 2007)

been noted for Siberian wetlands (Frey and Smith 2007). The wetland extent mapped by GLC 2000, which included JERS-1 mosaics as inputs, was 39 % of the LBA estimated area; this difference is likely a result of the lower resolution used for GLC 2000. The raster data set that most closely approximated the LBA wetlands estimate was GLWD-3 (wetlands area of 477×10^3 km^2, or 60 %). Open water area from the GLWD-1 and GLWD-2 vector data sets (108×10^3 km^2) exceeded the LBA high water estimate by 54 %; most of this is accounted for by areas mapped in the LBA data set as other types of wetland. Water areas mapped in the SRTM Water Body vector data set corresponded closely to the 1996 (high-water) LBA open water class, with a difference in total area mapped of 2 %. The Water Body data set is based on SRTM data acquired during February 2000, which corresponds to the middle of the rising water period for the mainstem Amazon.

Prigent et al. (2007) compared results of global coarse-resolution mapping of wetland dynamics using passive microwave and other satellite data sets to JERS-1-based wetlands mapping for the central Amazon (Hess et al. 2003). Extending this comparison to the full LBA wetlands study area covered by the GRFM mosaics, inundated area mapped by Prigent et al. (personal communication), averaged for May-June 1996, is 2.7×10^5 km^2, compared with a flooded area of 6.0×10^5 km^2 for the LBA high-water mosaic. The passive-based analysis provides high (monthly) temporal resolution and a long-term record; however, the coarse (0.25°) spatial resolution limits the ability to detect inundation outside of large wetlands and river floodplains, as shown in Fig. 6 (lower panel).

Applications for SAR-Based Wetlands Mapping

The LBA wetlands data set has been used in several studies to scale up from field measurements to regional estimates of components of the carbon cycle, including net primary productivity and turnover of aquatic macrophytes (Engle et al. 2008) and outgassing of CO_2 (Richey et al. 2002; Abril et al. 2013) and CH_4 (Melack et al. 2004), results that have provided insight into the contribution of Amazonian wetlands to regional carbon cycling (Melack et al. 2009; Aufdenkampe et al. 2011; Melack 2015) and their vulnerability to climate change (Melack and Coe 2013). Management-related applications of the data set include those relating the abundance of fish or aquatic mammals to floodplain habitats (Arraut et al. 2010; Lobón-Cerviá et al. 2015), or reviewing the extent and conservation status of Amazonian wetlands (Castello et al. 2013; Junk 2013).

Although no L-band satellites operated between 1998 and 2006, L-band availability resumed with the launch of the PALSAR sensor on board Japan's Advanced Land Observing Satellite (ALOS) in January 2006, and continues with ALOS-2, launched in 2014. Major sources of error and uncertainty in the JERS-1-based mapping are likely to be reduced owing to sensor improvements such as PALSAR's dual-polarization mode and lower noise floor (Rosenqvist et al. 2007). Examples of PALSAR-based mapping of Amazonian wetlands for small regions include Hawes et al. (2012), Arnesen et al. (2013), and Ferreira-Ferreira et al. (2014). Owing to a PALSAR acquisition strategy targeting global wetlands (Rosenqvist et al. 2007; Lowry et al. 2009), methods used in the present study have the potential for broader application to further the goal of quantifying wetland extent, vegetation type, and inundation patterns over large regions.

Conclusion

This study presents the first moderately high-resolution, validated mapping of wetland extent, vegetation cover, and inundation state for the entire lowland Amazon basin. Wetlands constitute an area of 8.4×10^5 km^2, 77 % of which is covered by woody vegetation. For the two seasons mapped, corresponding to low-water and high-water stages for the Amazon River, the flooded portion varied from 34 to 75 %. The true extent of wetlands can be assumed to be greater than these estimates since flooding along low-order streams or during seasons not captured on the JERS-1 mosaics must be considered. Examined in the context of long-term precipitation and river stage records, maximum flooding extent in the southern part of the basin is likely to be greater than estimated here.

Comparison of our wetlands mapping with other data sets indicates that land cover data sets derived solely from 0.5- to 1.0-km AVHRR or MODIS imagery are likely to underestimate Amazon wetland extent by up to an order of magnitude, while inclusion of JERS-1 inputs in 1-km scale mapping (as in GLC 2000) or a synthesis of multiple data sources (as in GLWD) can yield estimates closer to those of fine-resolution mapping. Coarse-scale inundation estimates based on passive microwave and other inputs provide improved temporal resolution but significantly underestimate flooding extent from smaller rivers and wetlands.

These results document the unique capabilities of L-band SAR sensors such as JERS-1 for mapping tropical wetland extent and inundation over large regions. Methods used in this study have the potential for broader application to further the goal of quantifying wetland extent, vegetation type, and inundation patterns at global scales.

Acknowledgments JERS-1 imagery used in this analysis was provided by Japan's Aerospace Exploration Agency (JAXA) as part of its Global Rain Forest Mapping (GRFM) Project, and JERS-1 mosaics were provided by B. Chapman at Jet Propulsion Laboratory. We gratefully acknowledge C. Prigent and F. Papa for making global inundation data sets available. This work was funded by NASA under LBA-ECO investigations LC-07 and LC-32, and NNX10AB66G. D. Alsdorf provided helpful comments on an earlier version of the paper.

References

Abell R (2002) Conservation biology for the biodiversity crisis: a freshwater follow-up. Conservation Biology 16(5):1435–1437

Abril G, Martinez J-M, Artigas LF, Moreira-Turcq P, Benedetti MF, Vidal L, Meziane T, Kim J-H, Bernardes MC, Savoye N (2013) Amazon River carbon dioxide outgassing fuelled by wetlands. Nature 505: 395–398

Acreman M, Holden J (2013) How wetlands affect floods. Wetlands 33(5):773–786

Adam E, Mutanga O, Rugege D (2010) Multispectral and hyperspectral remote sensing for identification and mapping of wetland vegetation: a review. Wetlands Ecology and Management 18(3):281–296

Alsdorf D, Lettenmaier D, Vorosmarty C, NASA Surface Water Working Group (2003) The need for global, satellite-based observations of terrestrial surface waters. Eos, Transactions American Geophysical Union 84(29):269–280

Anonymous (2005) Documentation for the Shuttle Radar Topography Mission Water Body Data Files. http://dds.cr.usgs.gov/srtm/version2_1/SWBD/SWBD_Documentation/Readme_SRTM_Water_Body_Data.pdf

Arnesen AS, Silva TSF, Hess LL, Novo EMLM, Rudorff CM, Chapman BD, McDonald KC (2013) Monitoring flood extent in the lower Amazon River floodplain using ALOS/PALSAR ScanSAR images. Remote Sensing of Environment 130:51–61

Arraut EM, Marmontel M, Mantovani JE, Novo EMLM, Macdonald DW, Kenward RE (2010) The lesser of two evils: seasonal migrations of Amazonian manatees in the Western Amazon. J Zool 280(3):247–256

Aufdenkampe AK, Mayorga E, Raymond PA, Melack JM, Doney SC, Alin SR, Aalto RE, Yoo K (2011) Riverine coupling of biogeochemical cycles between land, oceans, and atmosphere. Frontiers in Ecology and the Environment 9(1):53–60

Bayley PB (1995) Understanding large river-floodplain ecosystems. BioScience 45:153–158

Câmara G, Souza RCM, Freitas UM, Garrido JCP (1996) SPRING: integrating remote sensing and GIS by object-oriented data modeling. Computers and Graphics 20(3):395–403

Castello L, McGrath DG, Hess LL, Coe MT, Lefebvre PA, Petry P, Macedo MN, Renó VF, Arantes CC (2013) The vulnerability of Amazon freshwater ecosystems. Conservation Letters 6(4):217–229

Chapman B, Siqueira P, Freeman A (2002) The JERS amazon Multi-Season Mapping Study (JAMMS): observation strategies and data characteristics. International Journal of Remote Sensing 23(7): 1427–1446

Cole JJ, Prairie YT, Caraco NF, McDowell WH, Tranvik LJ, Striegl RG, Duarte CM, Kortelainen P, Downing JA, Middelburg JJ, Melack JM (2007) Plumbing the global carbon cycle: integrating inland waters into the terrestrial carbon budget. Ecosystems 10(1):172–185

Costa MH, Oliveira CHC, Andrade RG, Bustamante TR, Silva FA, Coe M (2002) A macroscale hydrological data set of river flow routing parameters for the Amazon Basin. Journal of Geophysical Research 107(D20), doi:10.1029/2000JD000309

Di Gregorio A (2005) Land cover classification system: classification concepts and user manual. Food and Agriculture Organization of the United Nations, Rome

Downing JA (2009) Global limnology: up–scaling aquatic services and processes to planet Earth. Internationale Vereinigung für Theoretische und Angewandte Limnologie: Verhandlungen 30: 1149–1166

Earth Satellite Corporation (2002) GeoCover product™ description sheet, http://glcf.umd.edu/library/guide/GeoCover_circa_1990_Product_Description.pdf

Engle DL, Melack JM, Doyle RD, Fisher TR (2008) High rates of net primary production and turnover of floating grasses on the Amazon floodplain: implications for aquatic respiration and regional CO_2 flux. Global Change Biology 14(2):369–381

Eva HD, de Miranda EE, Bella CMD, Gond V, Huber O, Sgrenzaroli M, Jones S, Coutinho A, Dorado A, Guimaraes M, Elvidge C, Achard F, Belward AS, Bartholome E, Baraldi A, Grandi GD, Vogt P, Fritz S, Hartley A (2002) A vegetation map of South America. Joint Research Centre of the European Commission, Luxembourg

Evans TL, Costa M, Telmer K, Silva TS (2010) Using ALOS/PALSAR and RADARSAT-2 to map land cover and seasonal inundation in the Brazilian Pantanal. IEEE Journal of Selected Topics in Applied Earth Observations and Remote Sensing 3(4):560–575

Farr TG, Rosen PA, Caro E, Crippen R, Duren R, Hensley S, Kobrick M, Paller M, Rodriguez E, Roth L, Seal D, Shaffer S, Shimada J, Umland J, Werner M, Oskin M, Burbank D, Alsdorf D (2007) The shuttle radar topography mission. Reviews of Geophysics 45(2). doi: 10.1029/2005RG000183

Ferreira-Ferreira J, Silva TSF, Streher AS, Affonso AG, de Almeida Furtado LF, Forsberg BR, Valsecchi J, Queiroz HL, de Moraes Novo EML (2014) Combining ALOS/PALSAR derived vegetation structure and inundation patterns to characterize major vegetation types in the Mamirauá Sustainable Development Reserve, Central Amazon floodplain, Brazil. Wetlands Ecology and Management:1–19

Finlayson CM, Valk AGvd (1995) Classification and inventory of the world's wetlands. Vegetatio 118 (Special issue (entire issue)):1–192

Finlayson CM, D'Cruz R, Davidson N (eds) (2005) Ecosystems and human well-being: wetlands and water. Millennium ecosystem assessment 2005. Millennium ecosystem assessment. World Resources Institute, Washington, D.C.

Frey KE, Smith LC (2007) How well do we know northern land cover? Comparison of four global vegetation and wetland products with a new ground-truth database for West Siberia. Global Biogeochemical Cycles 21:1–15

Friedl MA, McIver DK, Hodges JCF, Zhang XY, Muchoney D, Strahler AH, Woodcock CE, Gopal S, Schneider A, Cooper A, Baccini A, Gao F, Schaaf C (2002) Global land cover mapping from MODIS: algorithms and early results. Remote Sensing of Environment 83(1–2):287–302

Hansen MC, Potapov PV, Moore R, Hancher S, Turubanova S, Tyukavina A, Thau D, Stehman S, Goetz S, Loveland T (2013) High-resolution global maps of 21st-century forest cover change. Science 342:850–853

Hawes JE, Peres CA, Riley LB, Hess LL (2012) Landscape-scale variation in structure and biomass of Amazonian seasonally flooded and unflooded forests. Forest Ecology and Management 281:163–176

Hess LL, Melack JM, Simonett DS (1990) Radar detection of flooding beneath the forest canopy: a review. International Journal of Remote Sensing 11:1313–1325

Hess LL, Novo EMLM, Slaymaker DM, Holt J, Steffen C, Valeriano DM, Mertes LAK, Krug T, Melack JM, Gastil M, Holmes C, Hayward C (2002) Geocoded digital videography for validation of land cover mapping in the Amazon basin. International Journal of Remote Sensing 23(7):1527–1555

Hess LL, Melack JM, Novo EMLM, Barbosa CCF, Gastil M (2003) Dual-season mapping of wetland inundation and vegetation for the central Amazon basin. Remote Sensing of Environment 87:404–428

Hoekman DH, Vissers MA, Wielaard N (2010) PALSAR wide-area mapping of Borneo: methodology and map validation. IEEE Journal of Selected Topics in Applied Earth Observations and Remote Sensing 3(4):605–617

Jarvis A, Reuter HJ, Nelson A, Guevara E (2008) Hole-filled SRTM for the globe Version 4, available from the CGIAR-CSI SRTM 90 m Database, http://srtm.csi.cgiar.org

Josse C, Navarro G, Encarnación F, Tovar A, Comer P, Ferreira W, Rodríguez F, Saito J, Sanjurjo J, Dyson J, Celis ER, Zárate R, Chang J, Ahuite M, Vargas C, Paredes F, Castro W, Maco J,

Reátegui F (2007) Ecological systems of the Amazon basin of Peru and Bolivia: classification and mapping. NatureServe, Arlington

Junk WJ (2013) Current state of knowledge regarding South America wetlands and their future under global climate change. Aquatic Sciences 75(1):113–131

Junk WJ, Bayley PB, Sparks RE (1989) The flood pulse concept in river-floodplain systems. Canadian Special Publication of Fisheries and Aquatic Sciences 106:110–127

Junk WJ, Piedade MTF, Schongart J, Cohn-Haft M, Adeney JM, Wittmann F (2011) A classification of major naturally-occurring Amazonian wetlands. Wetlands 31:623–640

Kasischke ES, Melack JM, Dobson MC (1997) The use of imaging radars for ecological applications—a review. Remote Sensing of Environment 59:141–156

Keller M, Bustamante M, Gash J, Dias PS (2013) Amazonia and global change, vol 186. Wiley

Kingsford RT (2011) Conservation management of rivers and wetlands under climate change—a synthesis. Marine and Freshwater Research 62(3):217–222

Lamberti GA, Chaloner DT, Hershey AE (2010) Linkages among aquatic ecosystems. Journal of the North American Benthological Society 29(1):245–263

Landmann T, Schramm M, Colditz RR, Dietz A, Dech S (2010) Wide area wetland mapping in semi-arid Africa using 250-meter MODIS metrics and topographic variables. Remote Sensing 2(7):1751–1766

Lehner B, Döll P (2004) Development and validation of a global database of lakes, reservoirs and wetlands. Journal of Hydrology 296:1–22

Lobón-Cerviá J, Hess LL, Melack JM, Araujo-Lima CA (2015) The importance of forest cover for fish richness and abundance on the Amazon floodplain. Hydrobiologia 750:245–255

Loveland TR, Reed BC, Brown JF, Ohlen DO, Zhu Z, Yang L, Merchant JW (2000) Development of a global land cover characteristics database and IGBP DISCover from 1 km AVHRR data. International Journal of Remote Sensing 21(6):1303–1330

Lowry J, Hess L, Rosenqvist A (2009) Mapping and monitoring wetlands around the world using ALOS PALSAR: the ALOS Kyoto and Carbon Initiative wetlands products. In: Jones S, Reinke K (eds) Innovations in remote sensing and photogrammetry. Springer, Berlin, pp 105–120

Matthews E, Fung I (1987) Methane emissions from natural wetlands: global distribution, area, and environmental characteristics of sources. Glob Biogeochem Cycles 1:61–86

Melack JM (2004) Remote sensing of tropical wetlands. In: Ustin S (ed) Manual of remote sensing, vol 4. Wiley, New York, pp 319–343

Melack JM (2015) Aquatic ecosystems. In: Nagy L, Forsberg B, Artaxo P (eds.) The large-scale biosphere Atmosphere Programme in Amazonia. Ecological Studies, Springer

Melack JM, Coe MT (2013) Climate change and the floodplain lakes of the Amazon basin. Climatic change and global warming of inland waters: Impacts and Mitigation for Ecosystems and Societies: 295–310

Melack JM, Hess LL, Gastil M, Forsberg BR, Hamilton SK, Lima IBT, Novo EMLM (2004) Regionalization of methane emissions in the Amazon Basin with microwave remote sensing. Global Change Biology 10(5):530–544

Melack JM, Novo EM, Forsberg BR, Piedade MT, Maurice L (2009) Floodplain ecosystem processes. Amazonia and Global Change: 525–541

Mitchell TD, Jones PD (2005) An improved method of constructing a database of monthly climate observations and associated high-resolution grids. International Journal of Climatology 25(6):693–712

Nakaegawa T (2012) Comparison of water-related land cover types in six 1-km global land cover data sets. Journal of Hydrometeorology 13(2):649–664

Navarro G, Fuentes A (1999) Geobotánica y sistemas ecológicos de paisaje en el Gran Chaco de Bolivia. Revista Boliviana de Ecologia 5:25–50

Orodyne C, Friedl MA (2008) Using MODIS data to characterize seasonal inundation patterns in the Florida Everglades. Remote Sensing of Environment 112(11):4107–4119

Ozesmi SL, Bauer ME (2002) Satellite remote sensing of wetlands. Wetlands Ecology and Management 10(5):381–402

Peckham SD (2008) Geomorphometry in RiverTools. In: Hengl T, Reuter H (eds) Geomorphometry: concepts, software, applications. Elsevier, Amsterdam, pp 411–430

Prigent C, Papa F, Aires F, Rossow WB, Matthews E (2007) Global inundation dynamics inferred from multiple satellite observations, 1993–2000. Journal of Geophysical Research 112 (D12107). doi: 10.1029/2006JD007847

Revenga C, Campbell I, Abell R, Pd V, Bryer M (2005) Prospects for monitoring freshwater ecosystems towards the 2010 targets. Philosphical Transactions of the Royal Society B 360:397–413

Richey JE, Melack JM, Aufdenkampe AK, Ballester VM, Hess LL (2002) Outgassing from Amazonian rivers and wetlands as a large tropical source of atmospheric CO_2. Nature 416(6881):617–620

Rosenqvist A, Shimada M, Chapman B, Freeman A, De Grandi G, Saatchi S, Rauste Y (2000) The Global Rain Forest Mapping Project—a review. International Journal of Remote Sensing 21(6–7):1375–1387

Rosenqvist A, Shimada M, Ito N, Watanabe M (2007) ALOS PALSAR: a pathfinder mission for global-scale monitoring of the environment. IEEE Transactions on Geoscience and Remote Sensing 45(11): 3307–3316

Scott DA, Jones TA (1995) Classification and inventory of wetlands: a global overview. Vegetatio 118:3–16

Shimada M, Itoh T, Motooka T, Watanabe M, Shiraishi T, Thapa R, Lucas R (2014) New global forest/non-forest maps from ALOS PALSAR data (2007–2010). Remote Sensing of Environment 155:13–31

Silva TSF, Costa MPF, Melack JM, Novo EMLM (2008) Remote sensing of aquatic vegetation: theory and applications. Environmental Monitoring and Assessment 140:131–145

Silva TSF, Costa MPF, Melack JM (2010) Spatial and temporal variability of macrophyte cover and productivity in the eastern Amazon floodplain: a remote sensing approach. Remote Sensing of Environment 114:1998–2010

Siqueira P, Hensley S, Shaffer S, Hess L, McGarragh G, Chapman B, Freeman A (2000) A continental-scale mosaic of the Amazon Basin using JERS-1 SAR. IEEE Transactions on Geoscience and Remote Sensing 38(6):2638–2644

Wang Y, Hess LL, Filoso S, Melack JM (1995) Understanding the radar backscattering from flooded and nonflooded Amazonian forests: results from canopy backscatter modeling. Remote Sensing of Environment 54:324–332

Wood EF, Roundy JK, Troy TJ, Van Beek L, Bierkens MF, Blyth E, de Roo A, Döll P, Ek M, Famiglietti J (2011) Hyperresolution global land surface modeling: meeting a grand challenge for monitoring Earth's terrestrial water. Water Resources Research 47, W05301. doi:10.1029/2010WR010090